Original Paper *Forma*, **17**, 253–274, 2002

Evolution towards the Solution of a Shape Optimization Problem

Kuniko SATAKE* and Hisao HONDA

Hyogo University, Kakogawa, Hyogo 675-0195, Japan
**E-mail address: satake@hyogo-dai.ac.jp*

(Received September 9, 2002; Accepted November 26, 2002)

Keywords: Bending Energy, Intermediate Pattern, Optimization Problem, Shape of Closed Curve, Vertex Dynamics

Abstract. In problems to find the minimum or maximum of a target function under given constraints, attention has been paid to the final solution. Processes leading to the solution are often not of interest. Here we examine the paths and their variations leading to the solution of an optimization problem of the shape of a closed curve in a plane. The problem we deal with is to find the smoothest curve among curves whose length and enclosed area are given. We use the method of vertex dynamics where behavior of vertex coordinates is described by simultaneous partial differential equations including a potential term. We obtain, through intermediate patterns consisting of five, four and three lobes, finally a pattern consisting of two lobes. In the process of the pattern change, we observe fusing lobes (two neighboring lobes merge into one), retracting lobes (a lobe is drawn back into a body) and their intermediate types. Mechanisms of fusion and retraction are discussed with respect to the minimum bending energy under the given constraints.

1. Introduction

There are many types of optimization problems, e.g., an isoperimetric problem to find a closed curve of a given perimeter that encloses the greatest area. In such problems, attention usually has been focused on the final shape of the optimal solution. For example, CANHAM (1970) has explained the biconcave discocyte of the red blood cell by the principle of least total curvature of the erythrocyte membrane under the condition of the constant surface area and volume. HELFRICH (1973) has formalized the problem of the shape of a vesicle (a closed bilayer film) as a conditional problem of variation. According to this formalization, a catalogue of the axisymmetric vesicle shapes has been presented (DEULING and HELFRICH, 1976) and static equilibrium configurations of the vesicle shapes have been examined (JENKINS, 1977). Transformation among different shape of vesicles has also been investigated (SEIFERT *et al*., 1991). However, in these investigations, attention has not been paid to intermediate shapes, but only to the final shapes.

In the present paper, we will investigate what intermediate shapes a given initial pattern takes in the process of reaching the optimum shape in the two-dimensional space.

The investigation of intermediate shapes is closely related to the production of glassware from molten glass, baking of a roll from kneaded dough, and making pottery from kneaded clay. Ingenuity in shape change of viscous materials has been accumulated empirically, but has not been considered systematically or mathematically. Continuous shape change including intermediate shapes should be extensively studied in the research field of "Science on form".

Consider a flexible wire of fixed length formed into a closed curve in the two-dimensional space so that the constraint of a fixed length of perimeter holds. In addition, a further constraint is to keep the area enclosed by the perimeter at a constant value. The flexible wire changes its shape so that the total bending energy becomes the minimum. Progression towards the final shape is examined by computer simulations. We use a method of vertex dynamics developed in materials physics for study of an aggregate of crystal domains of metal or alloy, or an aggregate of soap froths (NAGAI *et al.*, 1988, 1990; KAWASAKI *et al.*, 1989; FUCHIZAKI *et al.*, 1995; NAGAI and HONDA, 2001). A closed planar curve is approximated by a polygon consisting of vertices linked by straight segments. Movement of the vertices is described by simultaneous partial differential equations where forces at vertices are represented by partial differential coefficients of a potential with respect to position coordinates. The potential consists of terms of bending energy along the polygon, deviation from a given periphery length of the polygon, and deviation from a given area of the polygon. That is, vertices move so that the potential decreases under the condition of allowance of slight increase of the bending energy, slight deviations from the given periphery length, or slight deviations from the given enclosed area. For example, the polygon is temporally allowed to deviate slightly from the given periphery length in order to decrease the bending energy.

The Monte Carlo method has already been used for investigation of the process leading to the optimal state of the plane curve under the constraints on the peripheral length and the enclosed area (LEIBLER *et al.*, 1987; MORIKAWA and SAITO, 1994; MORIKAWA *et al.*, 1997). The Monte Carlo method involves random fluctuations, so results from this method should be evaluated after averaging procedures. On the contrary, the vertex dynamics used here gives deterministic results that are appropriate for our purpose to investigate intermediate shapes.

Although we expected the curve to show multifarious shapes along the process towards the final state, the shape of the curve typically undergoes only two changes of fusion and retraction and their intermediates. The closed curve consists of several lobes, and two neighboring lobes fuse into one lobe or a protruding lobe is retracted into a body.

2. Methods

2.1. Vertex dynamics

A closed curve are approximated by a chain consisting of many vertices linked by straight segments. We use a method of vertex dynamics that has been developed in materials physics. There is a series of vertices linked by straight segments forming a plane closed chain in viscous fluid. Behavior of vertex i is described by equations of motion as follows,

$$\eta \frac{\mathrm{d}\boldsymbol{x}_i}{\mathrm{d}t} = -\nabla_i U \quad (i = 1, \ \ldots, \ N) \tag{1}$$

where η is a coefficient of viscosity of the fluid and $\boldsymbol{x}_i$ is the position vector of vertex i. The chain contains N vertices. The equations do not have an acceleration term because vertices do not have mass. U is a potential and consists of four terms of U_L, U_S, U_l and U_D as follows,

$$U = k_L U_L + k_S U_S + k_l U_l + k_D U_D. \tag{2}$$

The length of perimeter L_0 and the enclosed area S_0 are given. U_L is a square of difference of the perimeter length from the given length of the perimeter (L_0). U_S is a square of difference of the area from the given area S_0. U_l is a deviation of respective length of segments from the standard segment length. U_D corresponds to a total bending energy along the chain. k_L, k_S, k_l and k_D are weight constants which are related with the modulus of elasticity in mechanics.

When L is the sum of the length of the segments ($\sum_j l_j$), S is the area that is enclosed by the segments, and l_i is the length of each segment, each term of the right-hand side of Eq. (2) is given as follows,

$$U_L = \left(L - L_0\right)^2 \tag{3}$$

$$U_S = \left(S - S_0\right)^2 \tag{4}$$

$$U_l = \sum_j \left(l_j - \frac{L_0}{N}\right)^2 \tag{5}$$

$$U_D = \frac{EI}{2} \sum_j \frac{l_{j-1}/2 + l_j/2}{R_j^2}. \tag{6}$$

U_D of Eq. (6) is an approximation of the bending energy $(EI/2)\int(1/R_j^2)\mathrm{d}s$ of a curved flexible wire by a series of segments as shown in Fig. 1. Here, s is distance along the curve. E is Young's modulus of elasticity of the wire, I is the moment of inertia, R_j corresponds to the radius of curvature at vertex j. l_j is the length of each line segment, that is, the distance between vertex j and vertex (j + 1). Vertex 0 and vertex (N + 1) correspond to vertex N and vertex 1, respectively, because vertex 1 and vertex N are neighbors with each other.

2.2. Non-dimensionalization

We use L_0 as a new length of unit to make Eq. (1) dimensionally homogeneous. Based on the new unit, the system will be rewritten throughout. Each variable is expressed with prime (′) based on the new unit and we get the following relations,

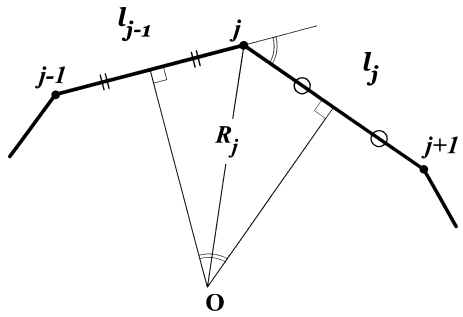

Fig. 1. A curve approximated by a chain of segments. Segment l_j links vertex j with vertex $j + 1$. Point O is the intersection of two perpendicular bisectors of segments l_{j-1} and l_j. R_j corresponds to the curvature radius at vertex j.

$$x_i = x_i' L_0, \quad L = L' L_0, \quad S = S' L_0^2,$$
$$l_j = l_j' L_0, \quad R_j = R_j' L_0, \quad S_0 = S_0' L_0^2.$$

Using these relations, Eq. (1) finally takes the form

$$\frac{\mathrm{d}x_i'}{\mathrm{d}t'} = -\frac{\partial}{\partial x_i'}(L'-1)^2 - k_S' \frac{\partial}{\partial x_i'}(S'-S_0')^2 - k_l' \frac{\partial}{\partial x_i'} \sum_j \left(l_j' - \frac{1}{N}\right)^2 - k_D' \frac{\partial}{\partial x_i'} \sum_j \frac{l_{j-1}'/2 + l_j'/2}{R_j'^2}.$$

In driving this equation, the following relations have been used.

$$t' = \frac{k_L t}{\eta}, \quad k_S' = \frac{k_S L_0^2}{k_L}, \quad k_l' = \frac{k_l}{k_L}, \quad k_D' = \frac{k_D EI}{2 k_L L_0^3}.$$

We should note that equation explicitly does not have a parameter corresponding to k_L. So we can reduce one parameter without loss of generality.

Hereafter, we omit prime (′) on the variables in the equation. After we perform the same procedure to the equation of $\mathrm{d}y_i/\mathrm{d}t$, we obtained following equations.

$$\frac{\mathrm{d}x_i}{\mathrm{d}t} = -\frac{\partial}{\partial x_i}(L-1)^2 - k_S \frac{\partial}{\partial x_i}(S-S_0)^2 - k_l \frac{\partial}{\partial x_i} \sum_j \left(l_j - \frac{1}{N}\right)^2 - k_D \frac{\partial}{\partial x_i} \sum_j \frac{l_{j-1}/2 + l_j/2}{R_j^2}, \quad (7)$$

$$\frac{\mathrm{d}y_i}{\mathrm{d}t} = -\frac{\partial}{\partial y_i}(L-1)^2 - k_S \frac{\partial}{\partial y_i}(S-S_0)^2 - k_l \frac{\partial}{\partial y_i} \sum_j \left(l_j - \frac{1}{N}\right)^2 - k_D \frac{\partial}{\partial y_i} \sum_j \frac{l_{j-1}/2 + l_j/2}{R_j^2}, \quad (8)$$

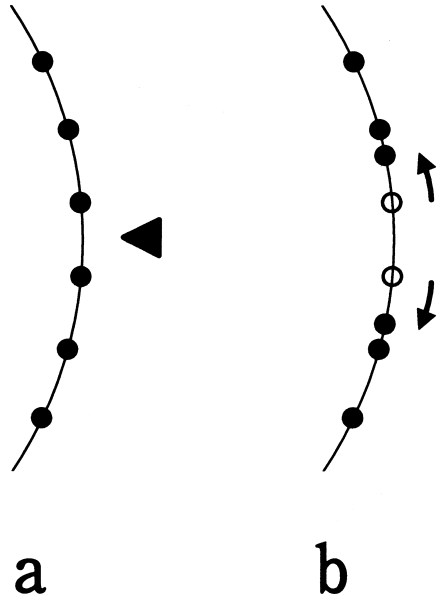

Fig. 2. Method to make an initiation of pattern change. A perturbation is given by elongation of a segment. Vertices are represented by solid circles. a) Arrowhead denotes a position where the perturbation is given. b) A segment is elongated by displacement of the two vertices. The two vertices move for 80% of the original segment length, respectively.

where $i = 1, ..., N$, and $\sum_j$ denotes the sum taken over $j = 1$ to N.

We carried out computer simulations with various values of parameters k_S, k_l and k_D. A reasonable pattern was obtained when $k_S = 1000$, $k_l = 10$ and $k_D = 1/6000$, where the second term and the third term in right-hand side of Eqs. (7) and (8) were similar order of values to that the first term (10^{-5}). That is, these three terms homogeneously contribute to the potential U. For the last term in Eqs. (7) and (8), when $k_D > 1/6000$, the bending energy of the system decreases in the process of simulations, but the pattern deviate greatly from the constrains on the perimeter length and the enclosed area. Such deviation does not occur when $k_D < 1/6000$. The larger the k_D value, the more sensitively the bending deformation contributes to the potential U. The large k_D value is preferable for our purpose. Then, we chose $k_D = 1/6000$ because of the largest k_D value within the k_D value that does not makes great deviation from the constrains.

The Runge-Kutta method (TOGAWA, 1981) was used for numerical calculations of Eqs. (7) and (8) with step size $h = 1 \times 10^{-6}$ to 1×10^{-4}.

2.3. Perturbation to make an initiation of pattern change

It is hard for patterns with high symmetry to change shape into another symmetrical pattern in simulations. We made an artificial perturbation, that is, we give to such patterns an initiation of deformation as shown in Fig. 2. Length of a selected segment was extended by displacement of the two neighboring vertices. The artificial perturbation raised the potential U by about 0.010.

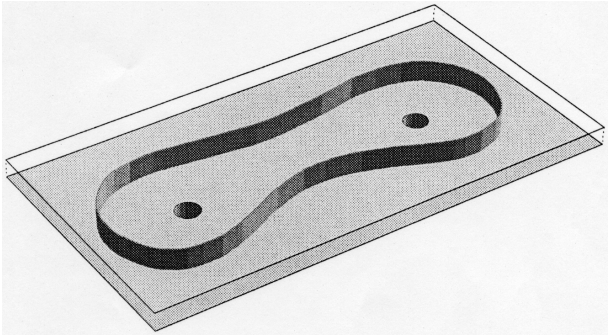

Fig. 3. Experiment of shape change of a closed loop of plastic tape by Brailsford. A closed loop of plastic tape is sandwiched between two parallel flat plates. There are two suction holes in the lower plate, and the pressure in the space enclosed by the loop and the two plates is reduced (based on figure 2 in BRAILSFORD, 1983).

2.4. Computers

A digital computer Alphaserver DS10 (Alpha processor, Digital UNIX V4.0F, Compaq Computer Corp., USA) was used for numerical calculation. Computer program was written by C-language and calculation was performed with double precision. Calculation was terminated when decreasing rate of U becomes smaller than 0.05% in the last 10,000 steps. A personal computer (PC/AT compatible, Pentium III 750 MHz processor, Windows98 SE, Takagi Industrial. Co., LTD., Sizuoka, Japan) was used for graphic display. Unix environment was introduced to Windows by a software cygwin (Red Hat Inc., USA, http://cygwin.com/). A graphic library glscwin was used, which is a Windows version of a graphic library GLSC (Graphic Library for Scientific Computing by Ryo Kobayashi, Daisuke Takahashi, Hiroshi Nakano, Junta Matsukidaira. ftp://ftp.st.ryukoku.ac.jp/pub/ryukoku/software/math/).

3. Results and Discussion

3.1. Experiment with a closed loop of plastic tape

In the present paper we dealt with the optimization problem what closed curve has the minimum bending under the restricted condition of given constant curve length and constant area enclosed by the curve. There was an experiment corresponding to this optimization problem. A closed loop of plastic tape was used in the experiment as shown in Fig. 3 (BRAILSFORD, 1983). The closed loop of plastic tape was sandwiched between two parallel flat plates. The upper plate was transparent. There were two suction holes in the lower plate, and the pressure in the space enclosed by the loop and the two plates was able to be reduced. The loop was sufficiently flexible so to decrease the enclosed area with the reduced pressure. The length of the loop does not change during the pressure reduction. When the pressure of the space was maintained constant, the shape of the loop is considered to become the shape with the minimum bending energy.

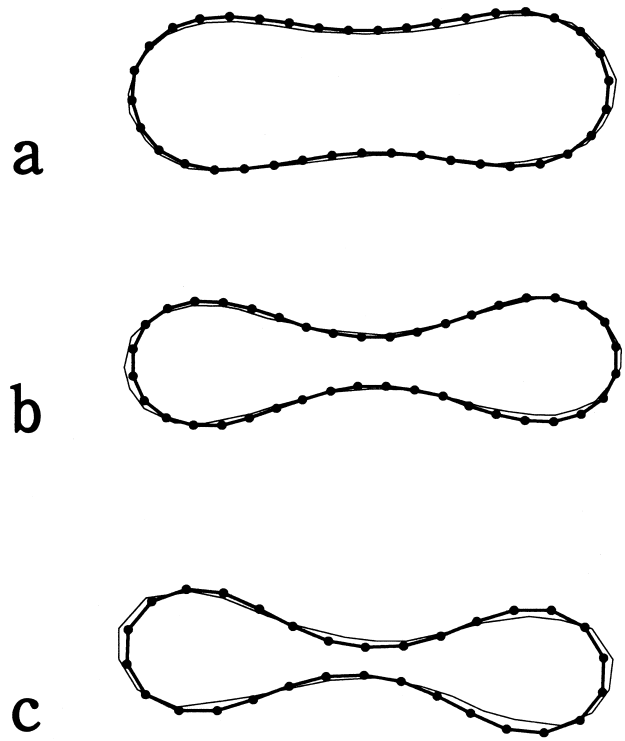

Fig. 4. Comparison of the shapes of the closed loop between the experimental result and the result by the computer simulation. The experimental results (thin line, after figure 3(a) in BRAILSFORD, 1983) are superposed with the results obtained by the computer simulations (thick line connecting points). Vertex number (N) in the computer simulation is 30. $h = 1 \times 10^{-4}$. Figures are normalized so that $L_0 = 1$. a) $S_0 = 0.04833$, simulation time (t) is 10; b) $S_0 = 0.03347$, $t = 100$; c) $S_0 = 0.02955$, $t = 1000$.

The experiment showed that the reduction of the pressure causes changes of the loop shape from a circle to an oval, then a pattern consisting of two lobes. Three patterns in the process of pressure reduction were reported (thin line in Figs. 4a–c). We investigated how closely we can simulate these experimental patterns by using the vertex dynamics which we described in "Methods".

The three patterns were respectively approximated by a polygon consisting of 30 vertices linked by segments of similar length. Coordinates (x_i, y_i) of vertices on the curves of the experimental results were obtained, and the total curve length and the area enclosed by the curve were calculated. The total curve length was normalized to be 1 ($=L_0$) by scaling. The area enclosed by the curve was S_0 after the normalization. The normalized pattern was used as an initial condition of the vertex dynamics, and we proceeded the process of decreasing U by the vertex dynamics. After many steps of the simulation the patterns did not change almost, which are shown in Fig. 4 (points linked by thick line).

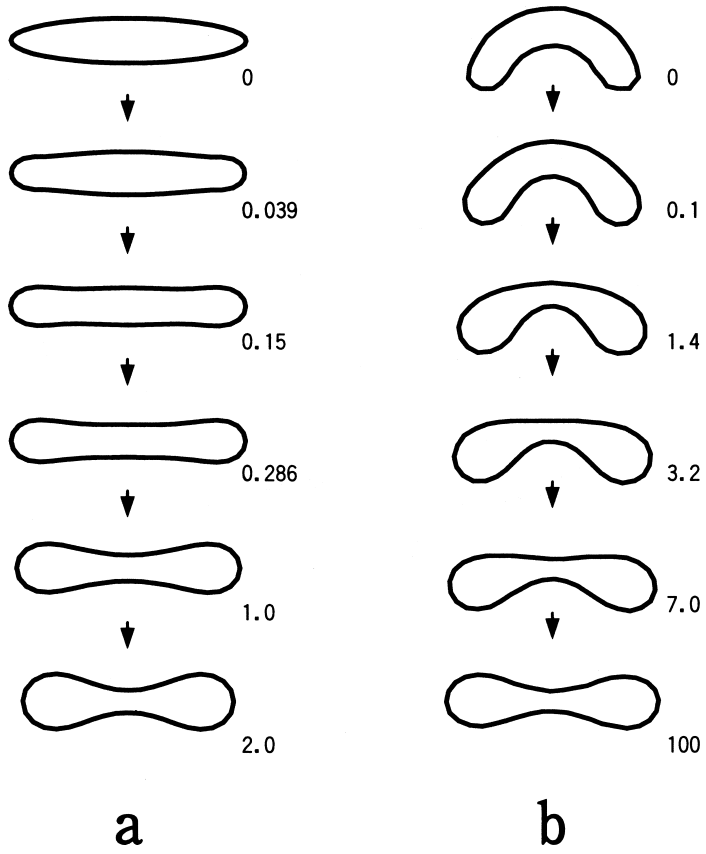

Fig. 5. Simulations with two different initial patterns. Each initial pattern has the same perimeter length L_0 = 1 and the same area S_0 = 0.0340. Vertex number (N) in the simulation is 40. Numerals are time (t) of the computer simulation. a) Shape change of an ellipse pattern. The ratio of minor axis to major axis is 0.189. $h = 1 \times 10^{-6}$. b) Shape change of a cup shaped pattern. The cup shape is enclosed by small and large semi-circles. The pattern is uniquely determined in mathematics when S_0 and L_0 are given. Forty vertices were arranged so that neighboring segments do not make sharp angle. $h = 1 \times 10^{-4}$.

The three patterns of different size (S_0) are shown in Figs. 4a–c. These patterns from the computer simulation (thick line with points) were close to the actual shapes (thin line). The result suggests that actual patterns by the experiment have the shape with the minimum bending energy. Among the three patterns (a, b and c), coincidence between the actual shape and the simulation result of pattern is not good for pattern c in comparison with patterns a and b. When curvature of the loop is large, thickness of the plastic tape may cause the discrepancy between the actual shape and the simulated pattern. For the simulations in the present paper, unless indicated otherwise, we use the restricted condition of constant perimeter length and area of the pattern of Fig. 4b (S_0 = 0.0340 and L_0 = 1).

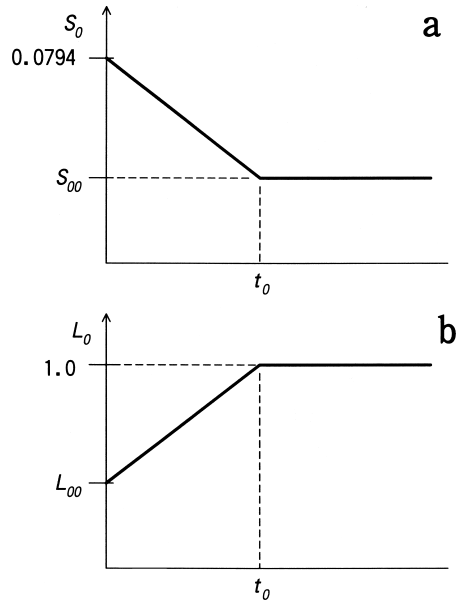

Fig. 6. Manners of changes of the area (S_0) and the perimeter length (L_0) in simulations with the initial conditions of circle. The initial condition (circle) changed its enclosed area or its perimeter length during computer simulations. a) The area enclosed by the perimeter (S_0) was linearly reduced from 0.07941 to S_{00}. The perimeter length was consistently maintained constant (L_0 = 1). After $t = t_0$, the area was maintained constant, S_{00}. b) The perimeter length (L_0) was increased from L_{00} to 1. The area was consistently maintained constant (S_0 = 0.0340). These two manners finally produced the same restricted condition as that of Fig. 4b (S_0 = 0.0340 and L_0 = 1).

3.2. Pattern change under the constrains on constant perimeter length and constant area

When the perimeter length and the area of the closed curve are fixed, we obtained the pattern consisting of two lobes having the minimum bending energy. The pattern was close to that by the experiment with the plastic tape. In general, only under the constrains on constant perimeter length and area, a closed curve shows multiple shapes. When the condition of the minimum bending energy is introduced, the pattern is defined. We examined whether or not typical two patterns with given perimeter length and area, an ellipse pattern and a cup shaped pattern change into the same pattern.

The top figure of Fig. 5a shows an approximated pattern of an ellipse (ratio of minor axis to major axis is 0.189) by a polygon consisting of vertices. The given perimeter length and the given area are the same as those of Fig. 4b. Figure 5a shows a sequential results of the simulation where numerals are time (t) of the computer simulation. As time passes, the elliptical pattern gradually swells at right and left protruding ends (t = 0.039), then, concaves at top and bottom (1.0), finally, it becomes a pattern consisting of two lobes (2.0).

Figure 5b shows a result obtained by the simulation started with a cap shaped pattern. Right and left ends swell gradually (t = 0.1). The upper convex curve is gradually flattened

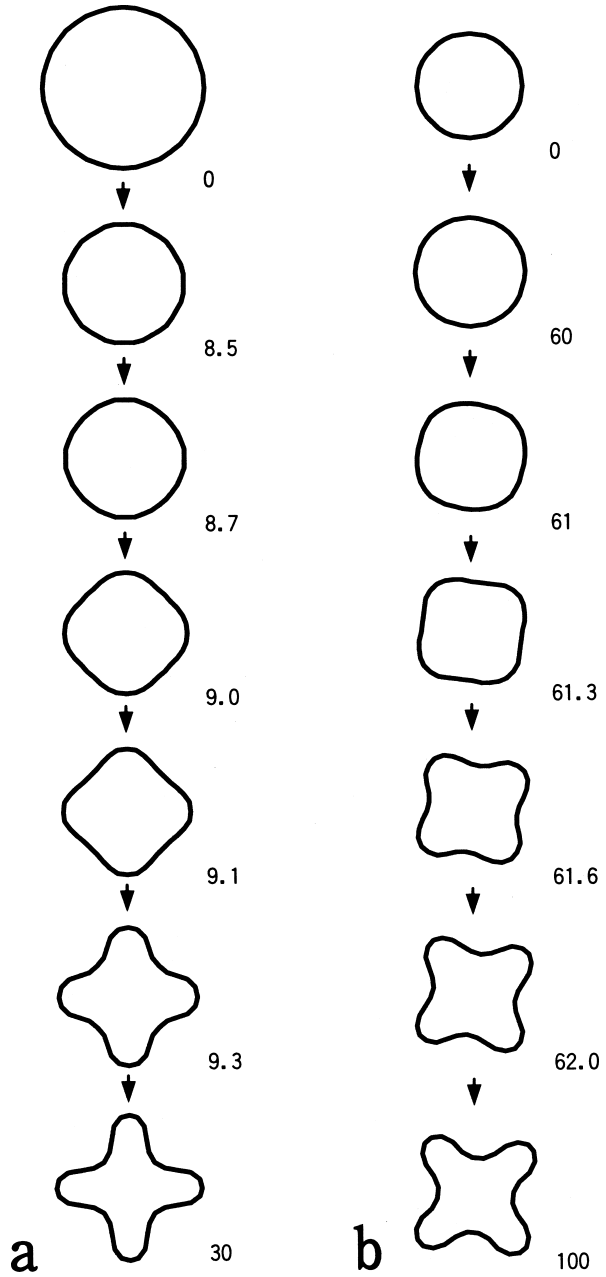

Fig. 7. Shape change simulation from a complete circle. a) The perimeter length was consistently maintained constant ($L_0 = 1$). The area S_0 was reduced as described in Fig. 6a ($S_{00} = 0.0340$. $t_0 = 10$). b) The area was consistently maintained constant ($S_0 = 0.0340$). The perimeter length was increased as described in Fig. 6b ($L_{00} = 0.6526$. $t_0 = 77.2$). Numerals are time (t) of the computer simulation. Vertex number (N) in the simulation is 40. Steps size of the simulation (h) is 1×10^{-4}.

(3.2), furthermore, it becomes concave (7.0). Finally the pattern has two hollows at top and bottom symmetrically, that is, the pattern consisting of two lobes (100.0).

An elongated pattern (ellipse) without concaves (Fig. 5a) and a pattern with one concave (Fig. 5b) both changed into the pattern with two lobes as the experimental pattern of Fig. 4b. These results suggest that multiple patterns with given constant perimeter length and constant area all become the same pattern consisting of two lobes under the condition of the minimum bending energy.

3.3. Shape change starting with a circle

Among closed curve patterns, a circle is the perfect symmetric shape and has the most homogeneous distribution of bending energy. Under the condition of the given constant perimeter length of closed curve, requirement of smaller area enclosed by the curve causes deviation from the perfect symmetry. How does this process proceed? We investigated two processes: reducing the area of a circle while the perimeter length is fixed and elongating the perimeter length of a small circle while the area is fixed.

For reduction of the area of a circle with the fixed constant perimeter length, the area was planed to be changed as shown in Fig. 6a. The perimeter length was consistently maintained constant ($L_0 = 1$). The area enclosed by the perimeter was linearly reduced to that of the experimental result of Fig. 4b ($S_{00} = 0.0340$), and then, maintained constant. Result of the computer simulation is shown in Fig. 7a.

Although the circle reduced its area under the constrain on constant perimeter length, it did not find a clue to break the symmetry. Thus, it was forced becoming a small circle ($t = 8.5$). After that, it becomes a square-like pattern with four round corners (9.0), and then, has four hollows (9.3), finally becomes a pattern consisting of four lobes (30).

Next, for elongation of the perimeter length to $L_0 = 1$ with the fixed constant enclosed area, the length was changed as shown in Fig. 6b. The perimeter length was linearly elongated from that of a complete circle ($L_{00} = 0.6526$) to the similar length of Fig. 4b (1.0), and then, maintained constant. The area was consistently maintained constant ($S_0 = 0.0340$).

Result of the computer simulation is shown in Fig. 7b. Although the simulation proceeded, the circle did not find a clue to break the symmetry ($t = 60$). After that, it becomes a square-like pattern with four round corners (61.3), and then, had four hollows (61.6), finally becomes a pattern consisting of four lobes (100).

The two computer simulations with the reduction of the circular area and the elongation of the circular perimeter length both resulted in the pattern with four lobes (Figs. 7a and 7b). Our vertex dynamics does not involve random numbers and is deterministic. Results from the vertex dynamics depended only on their initial conditions. The initial conditions for the simulation of Figs. 7a and 7b were circles, strictly speaking regular polygons with 40 corners, which were made using real numbers of double precision on Descartes rectangular x- and y-coordinates. The four-lobe patterns of Figs. 7a and 7b and the rectangular coordinates both have the same symmetry of 4-fold rotation. The patterns with four lobes are considered to be influenced by amplification of insignificant unbalance among numerals in the rectangular coordinates.

For confirmation of the thought, we performed computer simulations with an initial condition made by random numbers. We put 60 points at random along a circular curve and

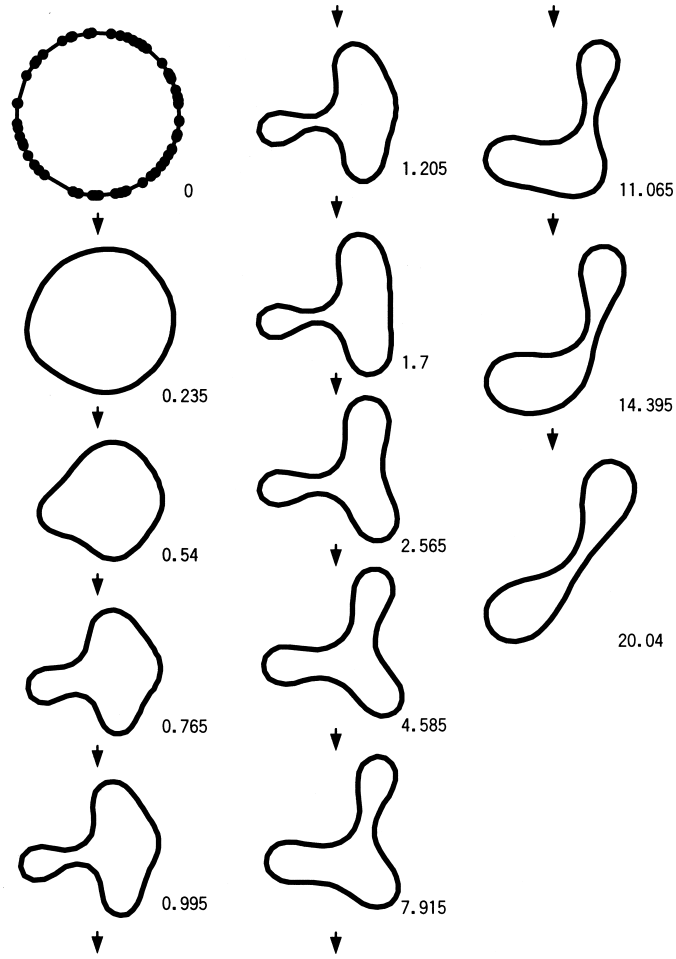

Fig. 8. Shape change simulation from a circle approximated by a segment chain of random length. The initial condition of a circle was made as follows. Vertices ($N = 60$) were distributed on a circular ring of perimeter length 1 by using uniform random number (radian) between 0 and 2π. The simulation was performed under the constrains that the perimeter length is consistently maintained constant and the area is reduced as the manner described in Fig. 6a (similar to Fig. 7a, except that $S_{00} = 0.03$ and $t_0 = 0.54$). Numerals are time (t) of the computer simulation. $L_0 = 1$. $h = 5 \times 10^{-6}$.

made an irregular polygon with 60 corners, which was used for the initial pattern in the computer simulation of reducing the circle area of Fig. 7a. We obtained various results, depending on series of random numbers, that is, circular patterns became the final pattern with two lobes via four lobe-like or three lobe-like patterns. One of the results is shown in Fig. 8. These results confirmed the thought that the procession of numerals of rectangular coordinates results in the four-lobe patterns in Figs. 7a and 7b.

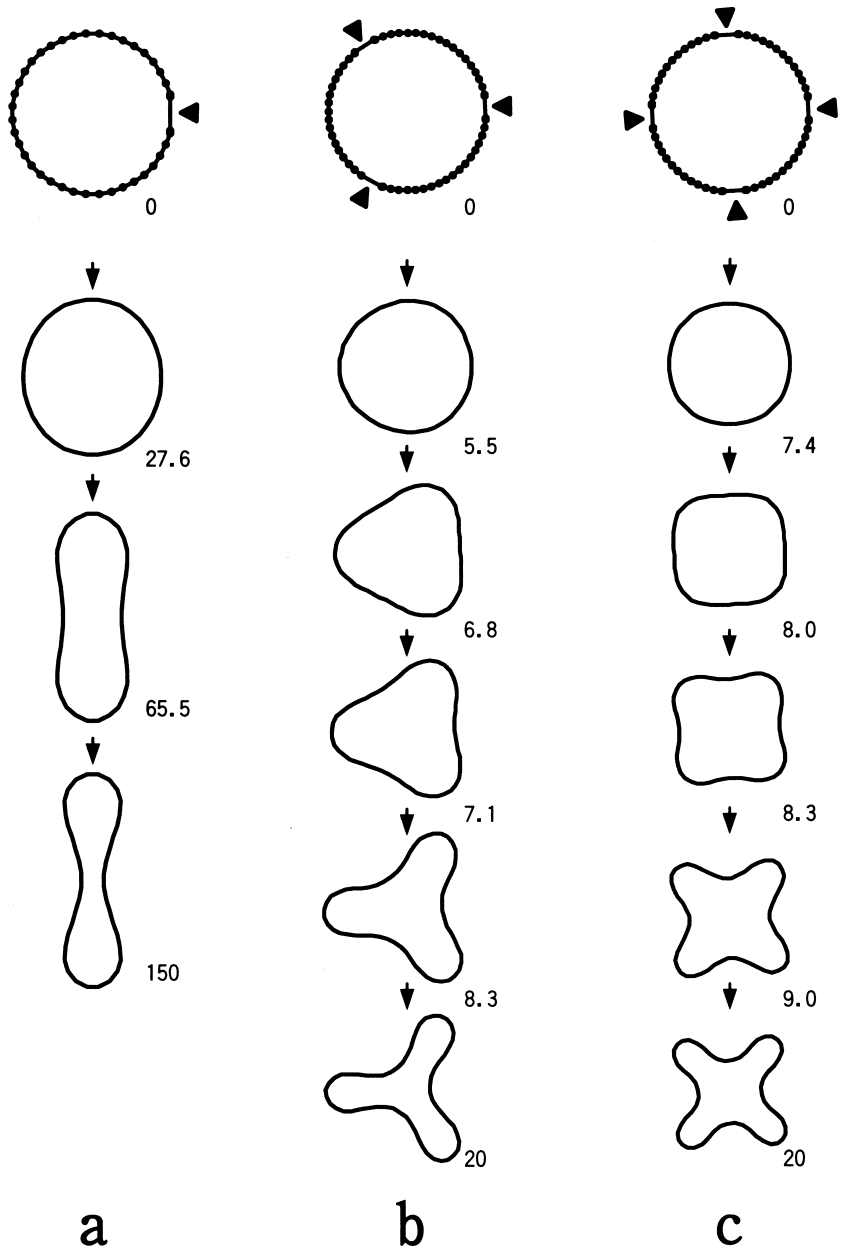

Fig. 9. Shape change simulations from circles with artificial perturbations. For initiation of the shape change, artificial perturbations as described in Fig. 2 were given. The area was reduced in a similar manner to Fig. 7a under the constrain on constant perimeter length. Number of the artificial perturbations was one (a), three (b) and four (c). Arrow heads denote positions of the artificial perturbation. The positions were defined in the rotational symmetry. Numerals are time (t) of the computer simulation. $h = 1 \times 10^{-4}$. The area is reduced as described in Fig. 6a. $S_{00} = 0.034$, $t_0 = 102.1$, $N = 40$ for a. $S_{00} = 0.03$, $t_0 = 10.9$, $N = 60$ for b and c.

Using the fact that the insignificant unbalances in the initial pattern makes the initiation of pattern change, we can promote prompt change of the shape by making artificial unbalance of vertex coordinates. We made an artificial initiation as follows.

3.4. Shape change of a circle with artificial perturbations

When the simulation was performed with the initial condition of the circle, it was hard for the circle to find a clue to break the circular symmetry (Figs. 7a and 7b). Here we introduce artificial perturbations for the initiation of shape change as shown in Fig. 2. Conditions of simulations were similar to that of Fig. 7a (the enclosed area, S_0 decreased as shown in Fig. 6a). Results of the simulation with one, three, four and five artificial perturbations were shown in Figs. 9a–c and 10.

When we added a single perturbation as shown in Fig. 9a (arrow head), the circle was elongated (t = 27.6), made two hollows (66.5) and became the two-lobe pattern (150). The position of the initial perturbation corresponds to one of the hollows.

When we add three perturbations in 3-fold rotational symmetry as shown in Fig. 9b (arrow heads), the circle became a triangle with round corners (6.8). The three edges of the triangle became concave (7.1), and finally the three-lobe pattern. The three positions of the initial perturbation correspond to the three hollows, respectively.

When we add four perturbations in 4-fold rotational symmetry as shown in Fig. 9c (arrow heads), the circle became a square with round corners (8.0). The four edges of the square became concave (8.3), and finally the four-lobe pattern. Similar to Figs. 9a and 9b, the four positions of the initial perturbation correspond to the four hollows, respectively.

When we add five perturbations in 5-fold rotational symmetry as shown in Fig. 10, the circle became a pentagon with round corners (t = 0.5). The five edges of the pentagon became concave (1.0), and then a five-lobe pattern (4.0). After that, it began to be deformed, through a pattern like four-lobe (7.0) and a three-lobe pattern (11), and finally the two-lobe pattern (150).

The above-mentioned simulations of Figs. 9 and 10 seem to show the three, four and five perturbations produce the three-, four-, and five-lobe patterns, respectively. However, five perturbations once produced the five-lobe pattern (t = 4 in Fig. 10), then it began to be deformed, through four-lobe (t = 7) and three-lobe patterns (11), finally, became the two-lobe pattern (150). Change of the potential U from the five-lobe pattern to the two-lobe pattern is shown in Fig. 11. The behavior of five-lobe pattern aroused a question whether or not, for example, we have a stable three-lobe pattern. We examined the value of potential U in detail. When we continued the simulation of the three-lobe pattern of Fig. 9b by the vertex dynamics, the values of U_L, U_S, U_l and U_D increased and decreased considerably, but the U value (the summation of U_L, U_S, U_l and U_D) almost kept at a constant. A numeral at 15th place of decimals of the U value sometimes increased by one and decreased by one around t = 20 (2×10^5 steps). Although the U value should not increase mathematically ($dU/dt \leq 0$, NAGAI and HONDA, 2001), the U value increased by one at 15th place of decimals. The fact shows that 15th place of decimals is out of bounds of the computation accuracy. When we continued the simulation furthermore, the U value did not increase, but decreased monotonically around t = 100. That is, the pattern went towards the two-lobe pattern. The three-lobe pattern of Fig. 9b had been searching for a way to reduce its U value on the bounds of computation accuracy.

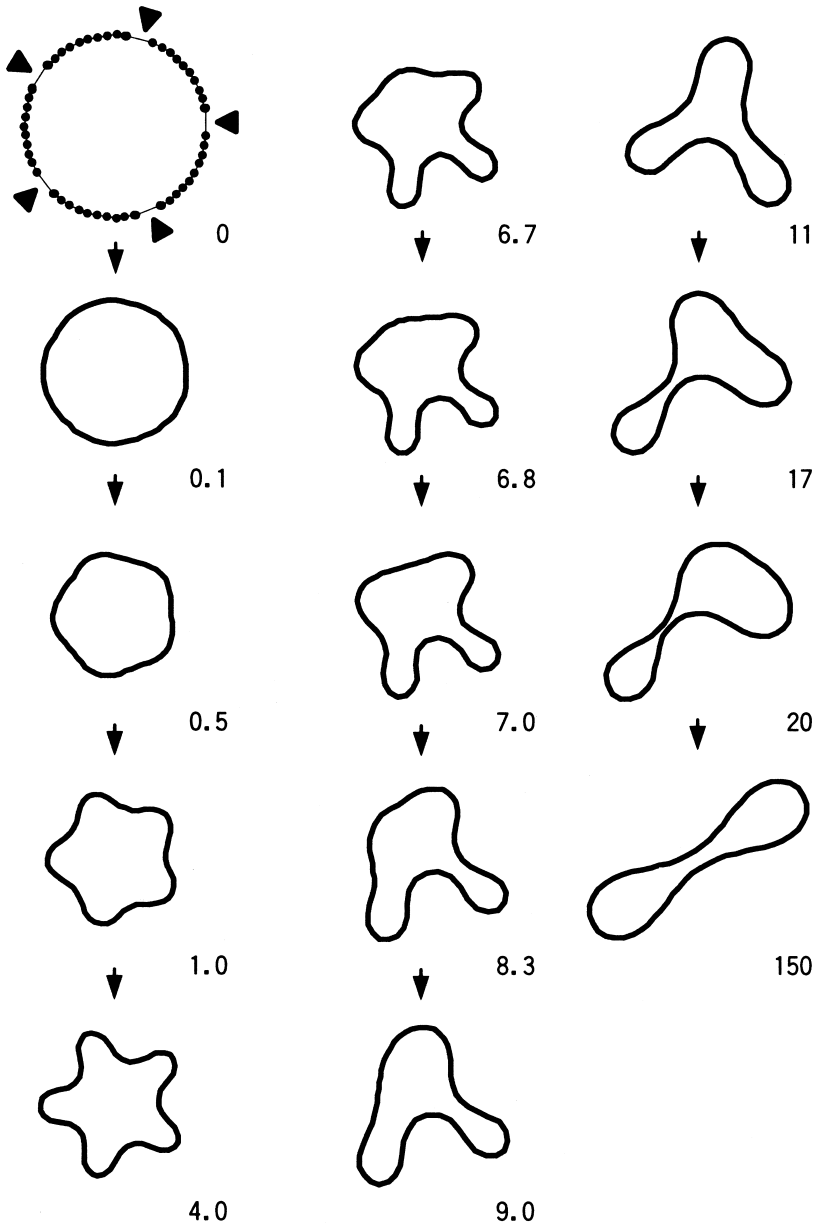

Fig. 10. A shape change simulation from a circle with five artificial perturbations. A computer simulation of the shape change from a circle was performed with five artificial perturbations. The condition was the same as Fig. 9, except that $S_{00} = 0.03$ and $t_0 = 0.10$.

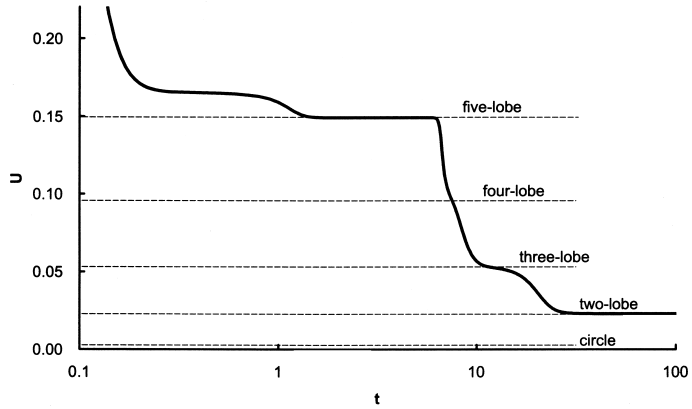

Fig. 11. Change of the potential U in the simulation from a circle with five artificial perturbations of Fig. 10. Abscissa, simulation time (t). Potential levels of the circle and the circle with five perturbations are 0.00651 and 0.0737, respectively. The potential level of the circle with five perturbations increases due to the reduction of the enclosed area until $t_0 = 0.10$ as shown in Fig. 6a. Potential levels of five-lobe (0.149), four-lobe (0.0959 in Fig. 7a), three-lobe (0.0535 in Fig. 9b), and two-lobe (0.0225 in Figs. 5a, 5b and 9a) are presented by broken lines.

The unstable three-lobe pattern is considered to be caused by insignificant unbalance in the process of shape change. Thus, we refined the three-lobe pattern with 3-fold rotational symmetry as completely as possible (Fig. 12). A simulation by the vertex dynamics was performed using the refined three-lobe pattern as an initial condition. When we continued the simulation until $t = 50$, we found that the values of U, U_L, U_S, U_l and U_D all do not change even at 15th place of decimals from $t = 2$ to 50 (almost 5×10^5 steps), that is, the pattern does not change any more by digital computation. We have a stable three-lobe pattern of closed curve in addition to the stable two-lobe pattern under the condition of computation accuracy with 15 places of decimals.

3.5. Shape change from the three-lobe pattern to the two-lobe pattern

The artificial perturbation can initiate shape change of the stable three-lobe pattern that had be made by refinement as described in Fig. 12. We were interested in intermediate shapes from the three-lobe pattern to the two-lobe pattern. A path to the two-lobe pattern is unique or varies? If it is not unique, how much does it vary? Since the vertex dynamics basically provides deterministic processes, it is appropriate to investigate variation of the path by the vertex dynamics.

We made the artificial perturbations at various sites of the three-lobe pattern as shown in Figs. 13a–e (arrow heads). The artificial perturbations were given at several sites from the bottom of a hollow between two lobes (Fig. 13a) to the top of a lobe (Fig. 13e). Results of the computer simulations are shown with time (t) in Figs. 13a–e.

When the perturbation was given at the bottom of a hollow between two lobes (Fig. 13a), the hollow having received the perturbation became shallow ($t = 24$). The two lobes fused into a fat lobe (30). Finally the two-lobe pattern appeared (100). The perturbation site

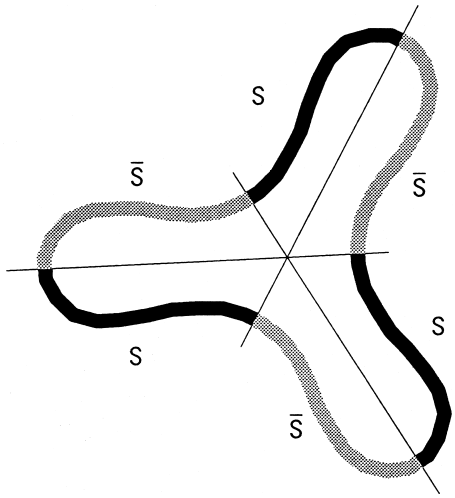

Fig. 12. Refinement of a three-lobe pattern with 3-fold rotational symmetry. The three-lobe pattern obtained by the simulation of Fig. 9b was divided into six parts, which are three "S" shaped (S) and three reflected "S" shaped ($\bar{S}$). The $\bar{S}$ patterns were reflected into their mirror image, and all six parts were rotated to be superposed into one "S" shape. Then, the averaged "S" shape was calculated. The six averaged "S" shape were inversely treated with operations of mirror and rotation to be reconstructed into a refined three-lobe pattern.

was going to be shifted towards the top of lobe. Figure 13b shows the two lobes far from the perturbation site fused with each other (t = 30 to 45). The fusion is not symmetric between the two lobes, but the lobe further from the perturbation site became dominant. Finally the two-lobe pattern was formed (200). Figure 13c shows, in contrast to Fig. 13b, the lobe far from the perturbation site retired (24 to 30). Next, Fig. 13d shows the lobe far from the perturbation site fused with the lobe received the perturbation (24). When the perturbation was given at the top of a lobe (Fig. 13e), the lobe receiving the perturbation itself retired.

On the basis of observations of these various changes from the three-lobe pattern to the two-lobe pattern, we can divide them into two groups, fusion of two lobes into one as shown typically in Fig. 13a, and retraction of a lobe to the main body as shown typically in Fig. 13e. We will call them fusion type and retraction type, respectively. The fusion type showed a characteristic properties that the connection between the fused large lobe and the third lobe became extremely narrow after fusion (e.g. indicated by $*$ in Fig. 13a), while the retraction type did not (see Fig. 13e). The shape changes in Figs. 13b–d were intermediate types between fusion and retraction. However, when we pay attention to a connection between the lobe by fusion and the third lobe, the connections of Fig. 13b (t = 45) and d (t = 30) are narrow (indicated by $*$) and the connection of Fig. 13c (t = 30) is not narrow (indicated by $*$). Thus, we can say that Figs. 13b and d rather belongs to the fusion type and Fig. 13c to the retraction type. It is concluded that the shape change from the three-lobe pattern to the two-lobe pattern contains the fusion types and the retraction type.

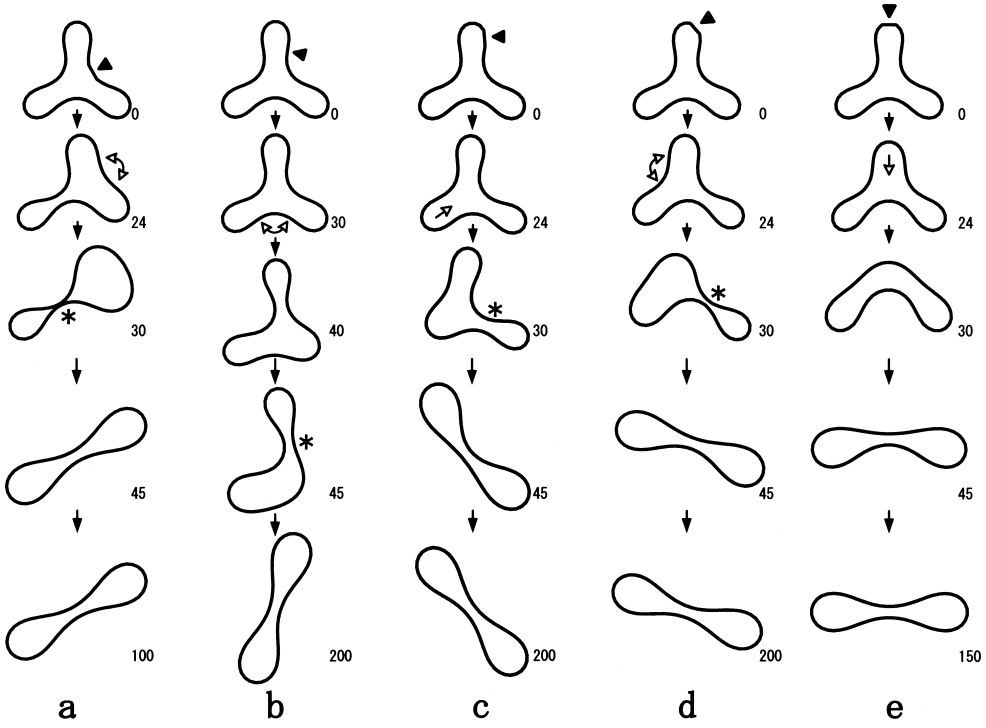

Fig. 13. Shape Change simulations from the three-lobe pattern to the two-lobe pattern. The initial pattern was the refined three-lobe pattern made from the pattern of Fig. 9b (t = 20) by the method of Fig. 12. Positions of the artificial perturbation were shifted from a concaved part between lobes to a protruded part (a–e). Arrow heads denote positions of the artificial perturbation. Open arrows denote positions of fusion or retraction. ∗ denotes narrow parts after fusion. Numerals are time (t) of the computer simulation. Vertex number (N) is 60. $L_0 = 1$, $S_0 = 0.03$, and $h = 1 \times 10^{-4}$.

When a pattern changes from the three-lobe one to the two-lobe one, the potential U decreases from 0.0535 to 0.0225. The potential U consisted of U_L, U_S, U_l and U_D as shown in Eq. (2). The decrease of U was mainly caused by the decreases of the deviation of the perimeter length U_L (=$(L - L_0)^2$) and the total bending energy U_D, since the decreases of U_S and U_l were small (5×10^{-7} and 1.6×10^{-4}, respectively). The potential U was three-dimensionally presented as a function of L and U_D as shown in Fig. 14a. The shape changes of the fusion type (Fig. 13a) and the retraction type (Fig. 13e) were presented by thick and thin lines, respectively. The potential U was also presented as a function of L (Fig. 14b) and a function of U_D (Fig. 14d), respectively. Figure 14c shows the correlation between L and U_D during the decrease of U. In the shape changes of the fusion and retraction types both, L decreased further deviating from 1 once, and returned to 1 according as becoming the two-lobe pattern. However, temporal deviation of L from 1 of the retraction type (thin line) was larger than that of the fusion type (thick line). For decrease of U, L should be close to

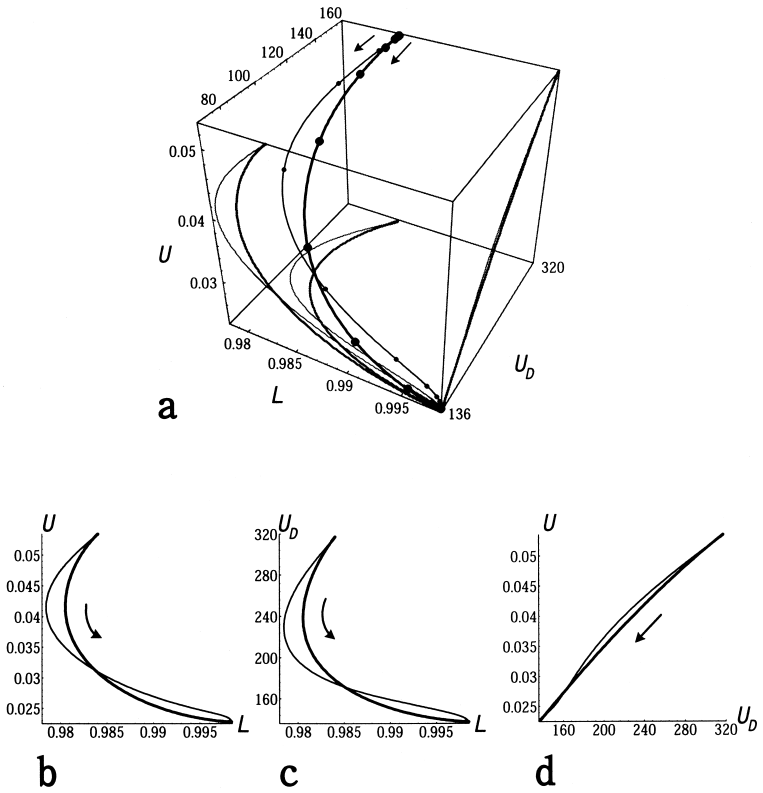

Fig. 14. Paths of shape change from the three-lobe pattern to the two-lobe pattern. a) Potential U is three-dimensionally presented as a function of the perimeter length L and bending energy U_D. b) Projection of a on L-U plane. c) Projection of a on L-U_D plane. d) Projection of a on U_D-U plane. Thick line represents the shape change of the fusion type of Fig. 13a. Thin line represents the shape change of the retraction type of Fig. 13e.

1. The reason why L deviated from 1 is because, on those steps, the decrease of U_D was dominant for the decrease of U in comparison with the decrease of $(L - L_0)^2$. Indeed, degree of the decrease of U_D of the retraction type (thin line) was larger than that of the fusion type (thick line) as U decreased (Fig. 14d).

In conclusion, to decrease U in the shape change from the three-lobe pattern to the two-lobe pattern, the retraction type (thin line) reduced the bending energy allowing temporally increase of deviation of L from 1. In contrast, the fusion type (thick line) reduced the bending energy moderately keeping L as close to 1 as possible.

3.6. Shape change from the four-lobe pattern to the two-lobe pattern by way of the three-lobe pattern

We proceeded the pattern change from the three-lobe pattern to the two-lobe pattern by giving the artificial perturbations. Similarly we made the artificial perturbations at a few

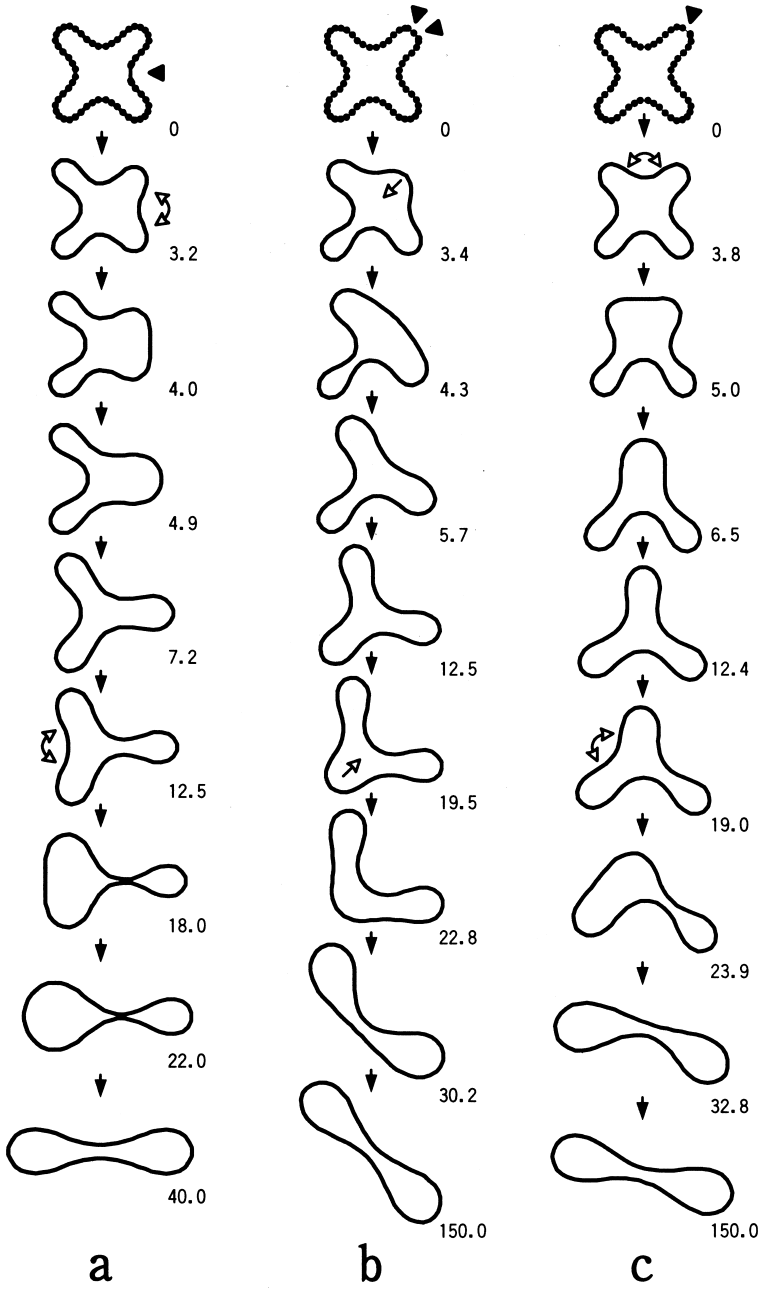

Fig. 15. Simulations of shape changes from the four-lobe pattern to the two-lobe pattern. a) One perturbation was given at the bottom of a hollow (a concave part between lobes). b) Two perturbations were given at the top of a lobe. c) One perturbation was given at the top of a lobe. Arrow heads denote positions of the artificial perturbation. Open arrow denotes position of fusion or retraction. Numerals are time (t) of the computer simulation. Vertex number (N) is 60. $L_0 = 1$, $S_0 = 0.03$, and $h = 4 \times 10^{-4}$.

sites of a four-lobe pattern. We observed the pattern change from the four-lobe pattern to the two-lobe pattern via the three-lobe pattern.

Figure 15a shows the result obtained by the simulation with a four-lobe pattern that had an artificial perturbation at the bottom of a hollow between two lobes. The two lobes forming the perturbed hollow began to fuse with each other (t = 3.2). Then, the pattern became three-lobe (7.2). The fusion occurred furthermore (12.5), finally the two-lobe pattern was made (40). Figure 15b shows the result of the simulation with the four-lobe pattern that had two artificial perturbations at the top of a lobe. One lobe which had received the perturbations in the four-lobe pattern retracted (3.4), then a three-lobe pattern was formed (12.5). After that, another retraction occurred (19.5), finally the two-lobe pattern was formed (150). Figure 15c shows the result of the simulation with the four-lobe pattern that had an artificial perturbation at the top of a lobe. Like the process of Fig. 15a, a fusion of two lobes was observed, but the fused two lobes were differed from those of Fig. 15a. The lobe received the perturbation fused with one of the neighboring lobes (3.8). Then, the pattern became three-lobe (12.4). After that, an asymmetric fusion took place (23.9). Finally the two-lobe pattern was formed (150).

The fusion and retraction types of shape change were observed not only in the shape change from the three-lobe pattern to the two-lobe pattern, but also in more general shape changes. Shape changes of the closed curves did not show multifarious types, but surprisingly a few, the fusion, retraction and their intermediate types. Furthermore, it should be noted that subtle differences of initial patterns determined the type of shape change.

4. Conclusion

When a shape with one of good symmetries transforms into one with another good symmetry, the degree of symmetry temporally decreases. Generally it is known that the path between the two good symmetries is not unique. What type of shape change it demonstrates and how many paths it has are exciting questions, but these have not been investigated intensively. In the present paper, with the aid of the method of the vertex dynamics that describes a deterministic evolution process, the shape change of the closed curve was investigated under the specified perimeter and area constraints.

It was elucidated that there are not many paths towards the optimal shape, but that the number of path types was extremely limited. For the closed curve in a plane evolving towards a state of the minimum bending energy under the conditions of keeping the peripheral length and the enclosed area constant, the shape change of the curve mainly consists of lobe-fusion and lobe-retraction.

The authors would like to thank Professor Kazushige Ishii (Nagoya University, Nagoya), Professor Tatsuzo Nagai (Kyushu Kyoritsu University, Kitakyushu), Associate Professor Tamiki Umeda (Kobe University of Mercantile Marine, Kobe), Professor Izumi Takagi (Tohoku University, Sendai), Professor Mitsugu Matsushita (Chuo University, Tokyo), Professor Ryuji Takaki (Tokyo University of Agriculture and Technology, Tokyo) and Dr. Akifumi Yuse (Hyogo University, Kakogawa, Hyogo) for valuable discussion.

REFERENCES

BRAILSFORD, J. D. (1983) Mechanoelastic properties of biological membranes, in *Membrane Fluidity in Biology, Vol. 1 Concepts of Membrane Structure*, pp. 291–319, Academic Press, Inc., San Diego.

CANHAM, P. B. (1970) The minimum energy of bending as a possible explanation of the biconcave shape of the human red blood cell, *J. Theor. Boil*., **26**, 61–81.

DEULING, H. J. and HELFRICH, W. (1976) The curvature elasticity of fluid membranes: a catalogue of vesicle shapes, *J. Phys. (Paris)*, **37**, 1335–1345.

FUCHIZAKI, K., KUSABA, T. and KAWASAKI, K. (1995) Computer modeling of three-dimensional cellular pattern growth, *Philosoph. Mag.*, **B71**, 333–357.

HELFRICH, W. (1973) Elastic properties of lipid bilayers: theory and possible experiments, *Z. Naturforsch*., **28c**, 693–703.

JENKINS, J. T. (1977) Static equilibrium configurations of a model red blood cell, *J. Math. Biol*., **4**, 149–169.

KAWASAKI, K., NAGAI, T. and NAKASHIMA, K. (1989) Vertex models for two-dimensional grain growth, *Philosoph. Mag*., **B60**, 399–421.

LEIBLER, S., SINGH, R. R. P. and FISHER, M. E. (1987) Thermodynamic behavior of two-dimensional vesicles, *Phys. Rev. Lett*., **59**, 1989–1992.

MORIKAWA, R. and SAITO, Y. (1994) Hard rod and frustum model of two-dimensional vesicles, *J. Phys. II France*, **4**, 145–161.

MORIKAWA, R., SAITO, Y. and HYUGA, H. (1997) Monte Carlo study of an axially symmetric vesicle, *J. Phys. Soc. Japan*, **66**, 2513–2520.

NAGAI, T. and HONDA, H. (2001) A dynamic cell model for the formation of epithelial tissue. *Philosoph. Mag*., **B81**, 699–719.

NAGAI, T., KAWASAKI, K. and NAKAMURA, K. (1988) Vertex dynamics of two-dimensional cellular patterns, *J. Phys. Soc. Japan*, **57**, 2221–2224.

NAGAI, T., OHTA, S., KAWASAKI, K. and OKUZONO, T. (1990) Computer simulation of cellular pattern growth in two and three dimensions, *Phase Transitions*, **28**, 177–211.

SEIFERT, U., BERNDL, K. and LIPOWSKY, R. (1991) Shape transformations of vesicles: Phase diagram for spontaneous-curvature and bilayer-coupling models, *Phys. Rev. A*, **44**, 1182–1202.

TOGAWA, H. (1981) *Method for Numerical Computation (Suuchi-keisanhou)*, Corona Publishing Co., Ltd., Tokyo, Japan (in Japanese).